
SCL-WC: Cross-Slide Contrastive Learning for Weakly-Supervised Whole-Slide Image Classification (Supplementary Materials)

Anonymous Author(s)

Affiliation

Address

email

1 Overview

The supplementary materials contain five aspects:

- Links to the datasets used in this work.
- Detailed experimental setups of our SCL-WC method.
- More visualization results for weak-supervised localization.
- More detailed results with standard deviation on these prostate datasets.
- A broader impact statement.

2 Data link

This work utilizes six datasets, where TCGA and PAIP are used for self-supervised pretraining, and the remaining four datasets (Camelyon 16, BRACS, PANDA, and DiagSet) are used for the weakly-supervised classification procedure. Links to these datasets are provided in Table 1.

Table 1: Links for datasets

Datasets	Link
Camelyon16	https://camelyon16.grand-challenge.org/
BRACS	https://research.ibm.com/haifa/Workshops/BRIGHT/
PANDA	https://panda.grand-challenge.org/
DiagSet	https://ai-econsilio.diag.pl
TCGA	https://portal.gdc.cancer.gov/projects
PAIP	http://www.wisepaip.org/paip

11

3 Experimental setups

All WSIs are first preprocessed with the Otsu method [1] to remove blank non-tissue regions at a magnification of $10\times$. In our self-supervised pretraining, the batch size is set to 2048 and each patch is encoded as a vector of length 768. Adam [2] optimizer with an initial learning rate of $1e-4$ is adopted. The learning rate is then scheduled by a cosine annealing scheme [3]. Our self-supervised pretraining is performed on a workstation with 48 Nvidia V100 cards. In our weakly-supervised classification procedure, each WSI is cropped into patches (224×224 pixels) with no overlap. The

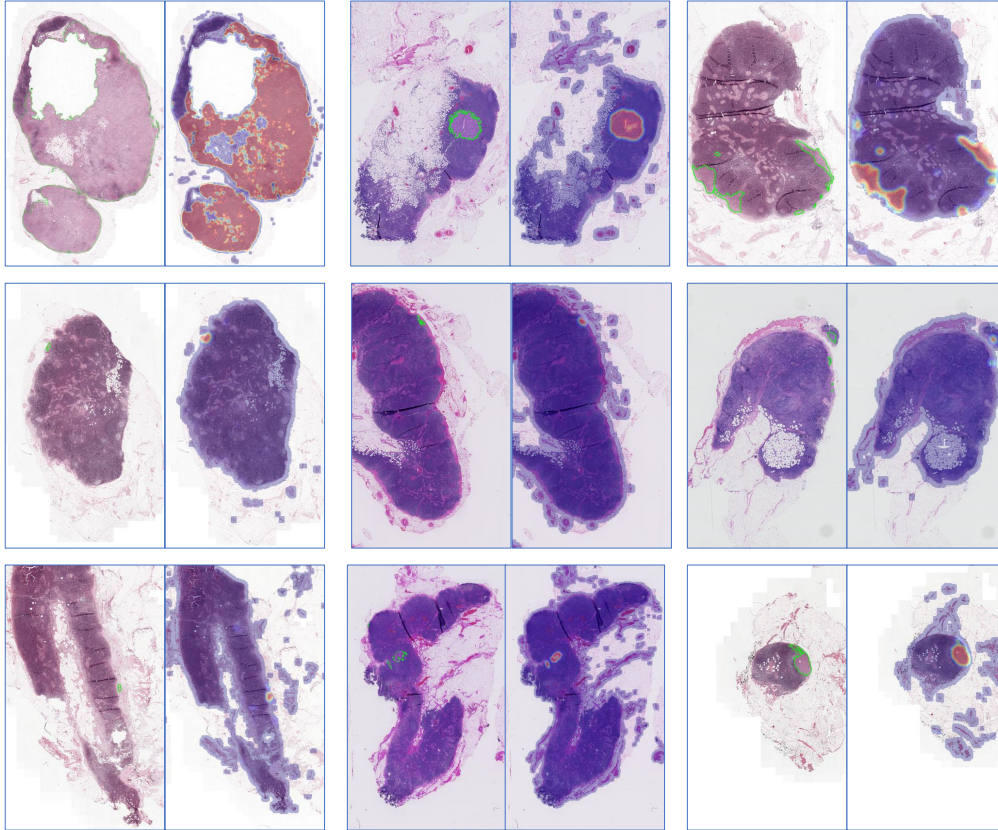


Figure 1: Visualization of weakly-supervised localization results. These samples are taken from the Camelyon16 dataset. In each image pair, the image on the left represents the ground truth of lesion regions marked with green lines and the image on the right is the results predicted by our model where these lesion regions are highlighted in warm colors.

19 batch size is set to 1 bag. Adam optimizer is employed with an initial learning rate of $1e-3$ (with
 20 cosine annealing) and a weight decay of $1e-5$. Following the previous contrastive learning method [4],
 21 the parameter τ is set to 0.07 in the WSCL. The two weight parameters (λ_1 and λ_2) in the \mathcal{L}_{CDA} are
 22 set to 0.8 and 0.2, respectively. The α , β , and γ in the \mathcal{L}_{total} are set to 1, 0.2, and 0.01, respectively.

23 4 Weakly-supervised localization results

24 We also provide more examples to demonstrate the localization performance of our weakly-supervised
 25 classification algorithm, which is shown in Figure 1. As shown in Figure 1, our SCL-WC method
 26 achieves excellent localization results even for small regional lesions.

27 5 Weakly-supervised classification results on the prostate datasets

28 We further provide detailed weakly-supervised classification results including means and standard
 29 deviations for two prostate datasets (PANDA and DiagSet), which are shown in Table 2.

30 6 Broader impact

31 Our histopathology-specific feature extractor is pretrained in a self-supervised manner on 15 million
 32 unlabeled patches, which guarantees data diversity and can be employed as an offline encoder for

Table 2: Results on the prostate datasets

	PANDA		DiagSet-A		DiagSet-B		DiagSet-C	
	ACC	AUC	ACC	AUC	ACC	AUC	ACC	AUC
Mean pooling	0.8407±0.0158	0.9386±0.0115	0.8313±0.0133	0.9237±0.0046	0.8197±0.0112	0.8914±0.0062	0.8478±0.0379	0.9159±0.0099
Max pooling	0.8847±0.0026	0.9508±0.0047	0.7330±0.0758	0.9315±0.0187	0.7377±0.0809	0.9371±0.0204	0.8695±0.0307	0.9489±0.0306
ABMIL [5]	0.8804±0.0127	0.9514±0.0048	0.7845±0.0346	0.9145±0.0192	0.8032±0.0426	0.9105±0.0251	0.8695±0.0106	0.9609±0.0208
TransMIL [6]	0.8715±0.0052	0.9408±0.0035	0.8290±0.0360	0.9290±0.0245	0.8246±0.0428	0.9334±0.0349	0.9130±0.0253	0.9669±0.0147
DSMIL [7]	0.8751±0.0122	0.9444±0.0046	0.7072±0.0691	0.9242±0.0175	0.8146±0.0824	0.9431±0.0161	0.8876±0.0162	0.9489±0.0182
CLAM [8]	0.8874±0.0060	0.9532±0.0050	0.7822±0.0122	0.9033±0.0129	0.8035±0.0133	0.9051±0.0146	0.8913±0.0173	0.9579±0.0166
Ours	0.9194±0.0034	0.9753±0.0038	0.8960±0.0109	0.9560±0.0159	0.9191±0.0236	0.9730±0.0123	0.9565±0.0134	0.9939±0.0034

33 various histopathological image applications, promoting the development of computational pathology.
34 Also, our proposed SCL-WC algorithm shows excellent flexibility and scalability, with great potential
35 to be extended to weakly-supervised localization and semi-supervised classification tasks. However,
36 our method should never be used for diagnosis alone, but only to assist pathologists in making faster
37 and better decisions by directly pointing out possible lesion regions. Future work will be dedicated to
38 conducting more clinical verification.

39 References

- 40 [1] N. Otsu, “A threshold selection method from gray-level histograms,” *IEEE transactions on*
41 *systems, man, and cybernetics*, vol. 9, no. 1, pp. 62–66, 1979.
- 42 [2] D. P. Kingma and J. Ba, “Adam: A method for stochastic optimization,” in *ICLR (Poster)*, 2015.
- 43 [3] I. Loshchilov and F. Hutter, “SGDR: Stochastic gradient descent with warm restarts,” in *ICLR*,
44 2017.
- 45 [4] X. Chen, S. Xie, and K. He, “An empirical study of training self-supervised vision transformers,”
46 in *ICCV*, 2021, pp. 9640–9649.
- 47 [5] M. Ilse, J. Tomczak, and M. Welling, “Attention-based deep multiple instance learning,” in *ICML*.
48 PMLR, 2018, pp. 2127–2136.
- 49 [6] Z. Shao, H. Bian, Y. Chen, Y. Wang, J. Zhang, X. Ji *et al.*, “TransMIL: Transformer based
50 correlated multiple instance learning for whole slide image classification,” *NeurIPS*, vol. 34,
51 2021.
- 52 [7] B. Li, Y. Li, and K. W. Eliceiri, “Dual-stream multiple instance learning network for whole
53 slide image classification with self-supervised contrastive learning,” in *CVPR*, 2021, pp. 14 318–
54 14 328.
- 55 [8] M. Y. Lu, D. F. Williamson, T. Y. Chen, R. J. Chen, M. Barbieri, and F. Mahmood, “Data-efficient
56 and weakly supervised computational pathology on whole-slide images,” *Nature biomedical*
57 *engineering*, vol. 5, no. 6, pp. 555–570, 2021.